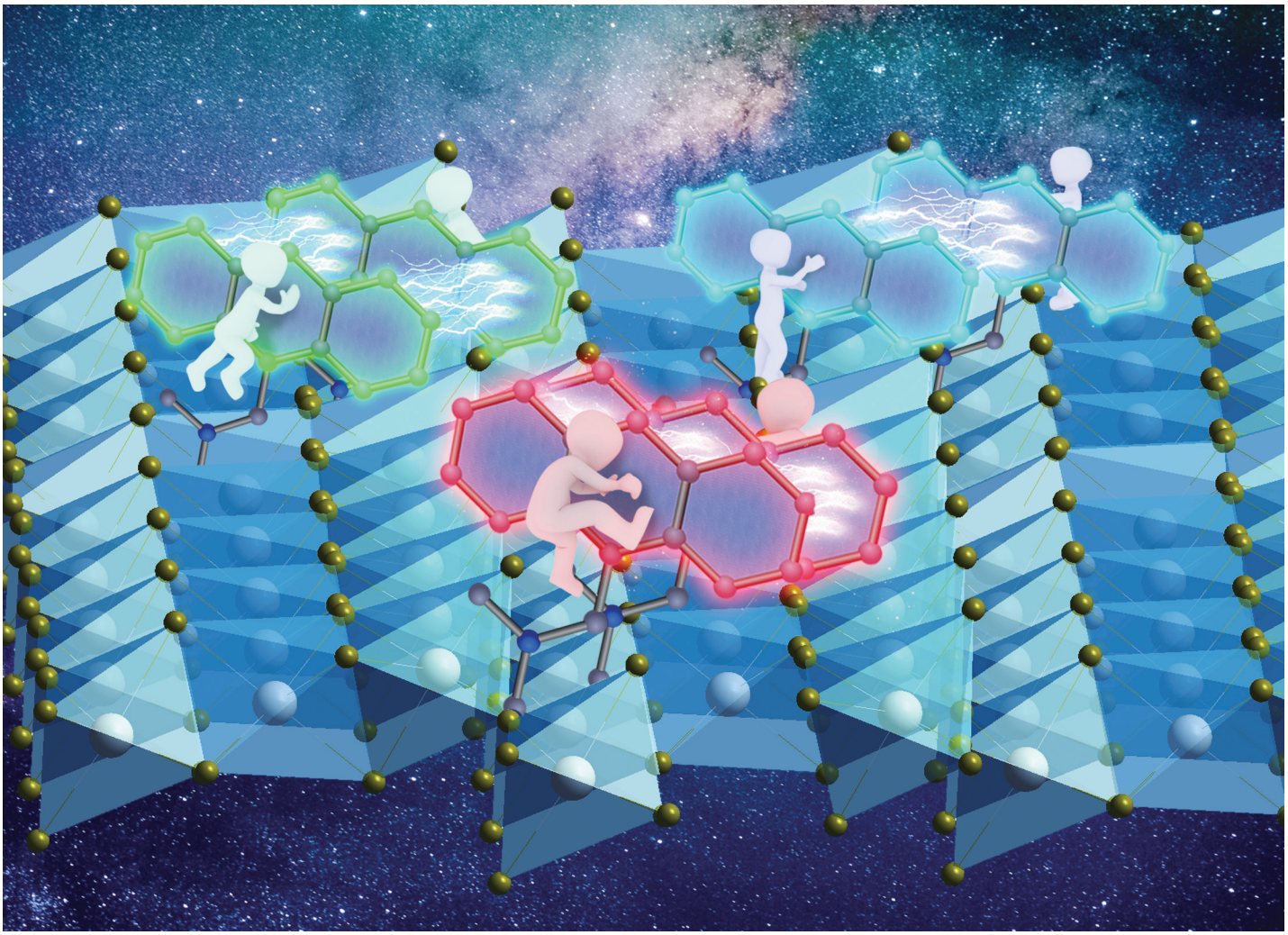

Showcasing research from Professor Binbin Luo's laboratory, School of Chemistry, Shantou University, Shantou, China.

Modulating anthracene excimer through guest engineering in two-dimensional lead bromide hybrids

Through varying the carbon chain length of guests, the stacking configuration of An dimers, including interplanar distance, overlap and intersection angle, is finely modulated, which allows a comprehensive understanding of the structure–properties relationship and excimer formation.

As featured in:

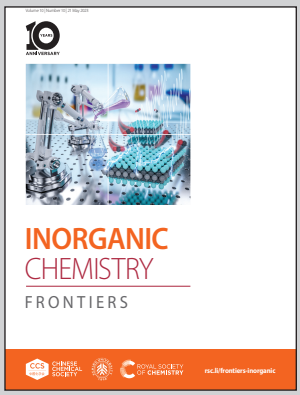

See Yan Kuai, Binbin Luo *et al.*, *Inorg. Chem. Front.*, 2023, **10**, 2917.

CCS 中国化学会 CHINESE CHEMICAL SOCIETY
PEKING UNIVERSITY 1898
ROYAL SOCIETY OF CHEMISTRY
rsc.li/frontiers-inorganic

INORGANIC CHEMISTRY FRONTIERS

RESEARCH ARTICLE

View Article Online
View Journal | View Issue

Cite this: *Inorg. Chem. Front.*, 2023, **10**, 2917

Modulating anthracene excimer through guest engineering in two-dimensional lead bromide hybrids†

Xiaohui Liu,‡[a] Xianli Li,‡[b] Jie Li,[a] Xin Lian,[a] Yonghong Xiao,[a] Ruosheng Zeng,[c] Shao-Fei Ni,[a] Ke Xu,[d] Yan Kuai,*[e] Wen-Xiu Ni[b] and Binbin Luo*[a]

A full understanding of the excimer formation and structure–property relationship is essential to their development in organic electronics. Herein, we propose a template strategy for finely modulating the stacking configuration of 9-dimethylaminomethyl-10-chloroanthracene (**DCAn**) dimers in two-dimensional (2D) (**DCAn**)$_4$Pb$_3$Br$_{10}$·2CH$_3$(CH$_2$)$_{X-1}$OH (**1-C*X***, $1 \leq X \leq 8$). By introducing alcohol guests with varied carbon lengths from methanol to octanol, **1-C*X*** with different stacking motifs of (anthracene) An dimers are obtained. The fine control on stacking parameters, including interplanar distance, overlap ratio, offset along long (d_x) and short (d_y) axis and intersection angle of An allows a deep insight into the key factors of excimer formation. The experimental and computational results confirm that the excimer interaction is strongly determined by the excimer types (anthracene or naphthalene) and interplanar overlap. An anthracene-type excimer is formed for **1-C*X*** ($6 \leq X \leq 8$) once d_x locates in the range of 1.08–1.23 Å, while **1-C*X*** ($1 \leq X \leq 5$) adopts the naphthalene-type excimer for $1.55 \leq d_x \leq 1.75$ Å. Due to the stronger anthracene-type excimer interaction, a great bathochromic shift of photoluminescence is observed for **1-C*X*** ($6 \leq X \leq 8$). Additionally, rod-like **1-C*X*** exhibits a high aspect ratio of ~72, thereby generating an excellent performance on optical waveguide with an optical loss coefficient of ~3 dB mm^{-1}. This work not only reveals the key factors on An excimer formation, but also provides an effective strategy for better understanding the structure–property of molecular excimers.

Received 15th February 2023,
Accepted 3rd April 2023

DOI: 10.1039/d3qi00289f

rsc.li/frontiers-inorganic

1. Introduction

Ever since the first discovery of the excimer fluorescence of pyrene by Förster and Kasper in 1954, the excimer emission of planar π-conjugated molecules has attracted increasing interest in organic electronics.[1–8] As a dimeric excited-state species, the excimer consists of a pair of an excited molecule and a ground-state molecule that interacts with each other through non-covalent dipole–dipole or coulombic interactions.[9–12] As a result, the formation of the aromatic excimer highly depends on the initial molecular conformation and stacking. Compared to the luminescent properties of monomers, aromatic excimer shows a structureless broadband emission with a large Stokes shift, which is greatly affected by intermolecular overlap and distance.[13,14] Although the strategies of molecular design and co-crystallization with the solvent have been developed to tune the configuration of dimers in molecular crystals, the concomitant factors, including spatial orientations, substituent groups (electron-donating or withdrawing), and solvent species bring complex and uncertain influence on the resulting optical properties. Moreover, these uncontrolled trial-and-error

[a]*Department of Chemistry and Key Laboratory for Preparation and Application of Ordered Structural Materials of Guangdong Province, Shantou University, Shantou 515063, P. R. China. E-mail: bbluo@stu.edu.cn*
[b]*Department of Medicinal Chemistry, Shantou University Medical College, Shantou 515041, P. R. China*
[c]*School of Physical Science and Technology, State Key Laboratory of Featured Metal Materials and Life-Cycle Safety for Composite Structures, Guangxi University, Nanning 530004, P. R. China*
[d]*Multiscale Crystal Materials Research Center, Shenzhen Institute of Advanced Technology, Chinese Academy of Sciences, Shenzhen 518055, P. R. China*
[e]*Information Materials and Intelligent Sensing Laboratory of Anhui Province, Anhui University, Hefei 230601, P. R. China. E-mail: yankuai@ahu.edu.cn*

†Electronic supplementary information (ESI) available: The experimental section, synthetic route of **DCAn**, crystal structure, crystal data, XRD, absorption, and PL spectra. CCDC 2240927 (**(DCAn)Br**), 2240928 (**1-C3**), 2240929 (**1-C5**), 2240930 (**1-C4**), 2240931 (**1-C2**), 2240932 (**1-C7**), 2240933 (**1-C1**), 2240934 (**1-C8**), 2240935 (**1-C9**), 2240936 (**1-C6**) and 2240942 (**DCAn**). For ESI and crystallographic data in CIF or other electronic format see DOI: https://doi.org/10.1039/d3qi00289f

‡X. Liu and X. Li contributed equally to this work.

approaches provide limited excimer modes to reveal key factors in the formation process of excimers. Therefore, it remains a great challenge to finely modulate the dimeric configuration for a deep understanding of structure–property relationship.

Low-dimensional metal halide hybrids (MHHs) have been intensively assembled with diverse organic cations for optoelectronic applications due to their unique band structure and outstanding optical properties.[15–24] As an anionic layer, the periodic and planar nature of the two-dimensional (2D) metal halide layer makes it a well-suited template for the ordered arrangement of organic cations, which is highly desirable for the deep understanding of molecular aggregates. Moreover, by engineering the band alignment between organic and inorganic layers, interlayer charge or energy transfer can be realized, resulting in distinct emissive behaviors. For instance, room temperature phosphorescence and triplet excimer emission of π-conjugated molecules are successfully observed through interlayer energy/electron transfer in 2D MHHs.[18,25–27] These results indicate that the anionic metal halide layer can function as a substrate for assembling π-conjugated cations to understand the structure–properties of molecular aggregates. Simultaneously, the presence of halogen ions provides enriched hydrogen binding sites for incorporating guest molecules, which can play the role of the modulator in controlling the dimeric configuration.

In this work, the anthracene (An) derivative 9-dimethylaminomethyl-10-chloroanthracene (**DCAn**) has been successfully synthesized and adopted as an organic countercation to construct 2D single-layered $(\mathbf{DCAn})_4Pb_3Br_{10}{\cdot}2CH_3(CH_2)_{X-1}OH$ (**1-C*X***, *X* represents the number of carbon atoms in alcohol guest). Due to the template effect of **1-C*X***, An dimers are orderly arranged and isolated through the interval of alcohol guests. By replacing with different alcohols (from methanol to octanol), the stacking configuration of An dimers, including the interplanar distance, overlap and intersection angles are finely modulated, which allows a comprehensive understanding of the structure–properties relationship and excimer formation.

2. Results and discussion

The synthesis of **DCAn** and corresponding bromide compound **(DCAn)Br** (Fig. S1†) was following the reported works with a small modification.[28] The single-crystal X-ray diffraction (SCXRD) shows that both **DCAn** and **(DCAn)Br** crystalize in monoclinic space group $P2_1/n$ with discrete pairwise anti-parallel-packed An dimer (Table S1 and Fig. S2†). The powder XRD patterns of **DCAn** and **(DCAn)Br** coincide well with that of the simulation (Fig. S2c and d†), confirming the high purity of these samples. Once **DCAn** and $PbBr_2$ are dissolved in alcohol and HBr mixed solvents, 2D single-layered **1-C*X*** with a monoclinic space group $C2/c$ (for $1 \le X \le 5$) or $P2_1/c$ (for $6 \le X \le 8$) were obtained and the corresponding crystal data are shown in Tables S2–S4.† Note that the diffraction data of **1-C6**, **1-C7**, and **1-C8** is obtained at 100 K due to the serious disorder of organic components. Similar to the crystal features of 2D Ruddlesden–Popper metal halide perovskites (MHPs),[20,29] **1-C*X*** show an alternating stacking of organic and inorganic layers (Fig. 1), which are coupled to each other through coulombic and hydrogen bonding interactions (Fig. S3†). Different from the corner-shared $[PbBr_6]$ octahedra in the layered MHPs, the Pb–Br inorganic layer of **1-C*X*** contains $[Pb_3Br_{12}]$ trimers of face-shared $[PbBr_6]$ octahedra linked through bridging Br to adjacent trimers (Fig. S4a†). Due to the highly distorted octahedra (Fig. S4b†), excitons are expected to easily interact with a lattice to generate self-trapped excitons.[30] Note that **1-C9** shows 1D chains comprising fully face-shared $[PbBr_6]$ octahedra (Fig. S5†). Such dimensional reduction is possibly due to the weakening of interlayer van der Waals interaction caused by the insertion of longer nonanol. As a result, a more stable 1D structure is preferred.

The host–guest structural features of **1-C1** highlight the important role of methanol guests in the configuration of An dimers, which inspired us to reveal the effect of alcohol guests on tuning the configuration of An dimers. Upon replacing methanol with other saturated linear alcohol species, the structural features of the inorganic layer remained except for the occurrence of interlayer slippage in van der Waals interfaces for accommodating longer alcohol guests. Unexpectedly, water guest is simultaneously implanted into monoclinic **1-C6**, **1-C7**, and **1-C8** with a different space group of $P2_1/c$ (Fig. 2), possibly attributed to the expanding space induced by the insertion of longer alcohol molecules (Fig. S6†). Compared to water-free samples, water molecules in **1-C6**, **1-C7**, and **1-C8** act as hydrogen-bond-mediators that strengthen the interplay between alcohol guests and hybrid hosts (Fig. S3b†).

Because of the template effect of the inorganic layer, discrete parallel-packed An dimers spaced by alcohol guests (Fig. 2) are obtained in **1-C*X***. With the increase in the number of carbon atoms in alcohol guests, the configuration of An dimers is greatly affected and the stacking parameters are shown in Table 1. As expected, the average interplanar distance (Table 1) of An dimers decreases gradually from 3.549 Å (**1-C1**) to 3.516 Å (**1-C5**) and then increases slightly from 3.440 Å (**1-C6**) to 3.463 Å (**1-C8**). Interestingly, a turning point of interplanar distance occurs from **1-C5** to **1-C6** (Fig. S7†). The initial reduction of interplanar distance is caused by the increasing volume of alcohol guests, while the subsequent increase is caused by the displacement of guests to the cavity surrounded by four dimers (Fig. 2h). Different from the alcohol guests with shorter lengths ($1 \le X \le 5$), the longer alcohol guests ($6 \le X \le 8$) insert into the adjacent organic layers (Fig. S6†), which expands the cavity between An dimers and induces the rotation of An dimers (Fig. 2e and f). Upon increasing the length of alcohol guests from hexanol to octanol, the inter-dimer cavity is too small to accommodate the guests including two alcohol molecules and one water molecule. As a result, the guests are forced to move into the cavity surrounded by four dimers.

Since the perpendicular distance of **1-C*X*** is close to 3.3 Å as in graphite, a typical π–π interaction is anticipated for these

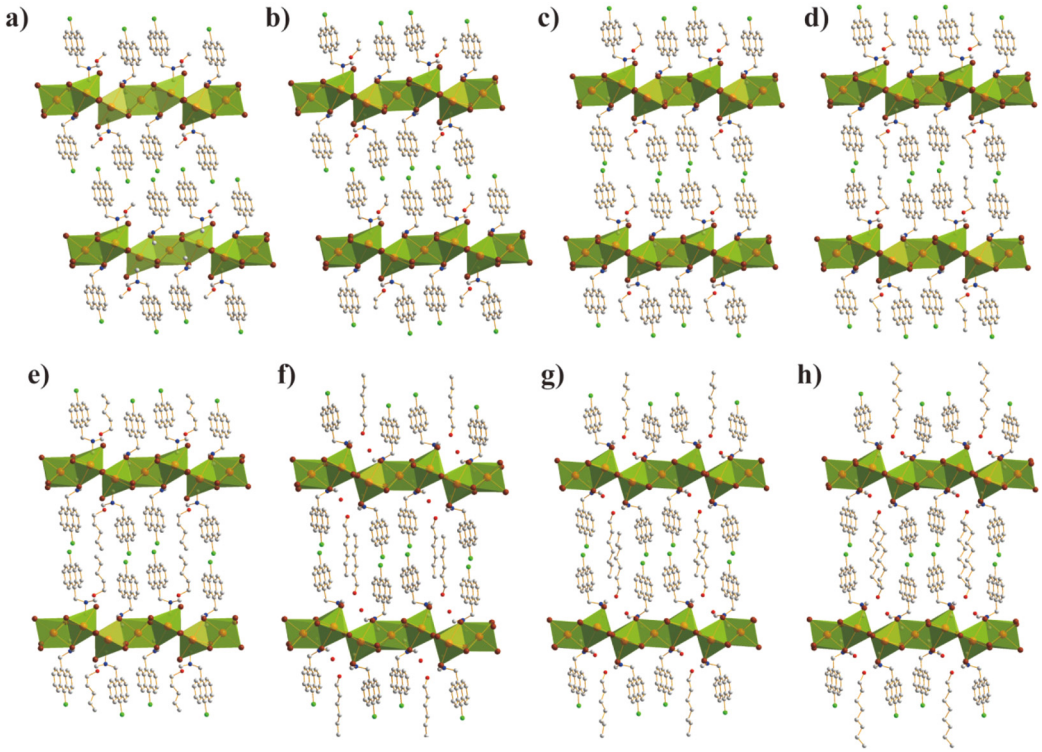

Fig. 1 Crystal structures of (a) **1-C1**, (b) **1-C2**, (c) **1-C3**, (d) **1-C4**, (e) **1-C5**, (f) **1-C6**, (g) **1-C7** and (h) **1-C8**. Pb (orange), Br (dark red), Cl (green), N (blue), O (red), and C (gray).

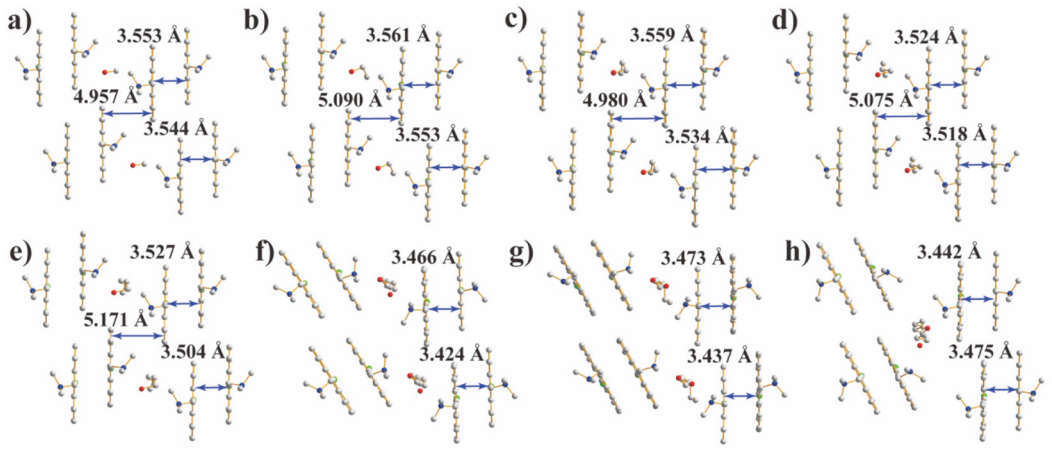

Fig. 2 Arrangement of **DCAn** cations in the organic layers of (a) **1-C1**, (b) **1-C2**, (c) **1-C3**, (d) **1-C4**, (e) **1-C5**, (f) **1-C6**, (g) **1-C7** and (h) **1-C8**. Cl (green), N (blue), O (red), and C (gray).

samples. Previous works have also shown that An dimers with such a distance range usually exhibit strong excimer interaction.[5,11,31–38] These series of **1-C*X*** samples with similar configurations allow a deep insight into the key factors that affect the excimer formation. The phase purity of all samples was determined by XRD (Fig. S8†), in which the diffraction peaks of all the samples coincide well with the simulated patterns. Note that the diffraction peaks of **1-C*X*** ($6 \leq X \leq 8$) obtained at room temperature (RT) shift by only ~0.1° towards lower angle direction compared to the corresponding simulated patterns obtained at 100 K, indicating the nearly identical structures of **1-C*X*** ($6 \leq X \leq 8$) at RT and 100 K.

Interestingly, the **1-C6** single crystal with a homogeneous distribution of all elements shows a rod-shaped morphology despite the 2D stacking feature of these samples (Fig. S9†). Upon 365 nm UV irradiation, rod-like **1-C*X*** presented guest-dependent emission tuning from cyan to yellow-green, indicating the significant effect of alcohol guests on the optical pro-

Table 1 Structural parameters and photophysical properties of **1-C*X***

Samples	Guest	Space group	Dimer configuration	d_x (Å)	d_y (Å)	Overlap (%)	$d_{\pi-\pi}$ (Å)	Intersection angle (°)	λ_{em} (nm)	PL QY (%)
DCAn	—	$P2_1/n$		0.608	1.360	31.3	3.583	0	567	8.8
(DCAn)Br	—	$P2_1/n$		1.469	0.981	45.0	3.540	0	515	1.6
1-C1	Methanol	$C2/c$		1.744	0.459	53.7	3.549	1.502	510	3.5
1-C2	Ethanol	$C2/c$		1.557	0.694	55.3	3.557	3.954	522	3.0
1-C3	Propanol	$C2/c$		1.663	0.817	47.8	3.547	3.438	506	7.1
1-C4	Butanol	$C2/c$		1.715	0.840	48.4	3.521	3.560	490	7.0
1-C5	Pentanol	$C2/c$		1.651	0.905	45.9	3.516	4.607	493	9.0
1-C6	Hexanol H_2O	$P2_1/c$		1.175	1.174	42.3	3.445	6.244	544	9.6
1-C7	Heptanol H_2O	$P2_1/c$		1.233	0.945	51.7	3.455	8.501	552	9.6
1-C8	Octanol H_2O	$P2_1/c$		1.081	1.065	44.9	3.459	8.742	550	15.4

perties of **1-C*X*** (Fig. 3). To reveal the underlying mechanism, UV-vis, and photoluminescence (PL) spectra were conducted as shown in Fig. S10† and Fig. 3. The absorption spectra of both **DCAn** and **(DCAn)Br** methanolic solutions show fine-structured bands from 325 to 400 nm (Fig. S10a and b†), which are assigned to the π–π* transition of the An core.[39] Correspondingly, identical emissive behavior with peaks at 405, 426, 450, and 482 nm generated from the **DCAn** monomer is observed for **DCAn** and **(DCAn)Br** methanolic solutions. Different from the optical properties of monomers in the solution, solid-state **DCAn** and **(DCAn)Br** containing isolated An dimers show an absorption step at ~450 nm and a broadband emission centered at 567 and 515 nm (Fig. S10c and d†), respectively. With respect to the PL of methanolic solution, such a great bathochromic shift is caused by the strong An excimer interaction in the solid state.

In accordance with the UV-vis spectra of **DCAn** and **(DCAn)Br** powders, similar absorption behavior with an onset at ~450 nm is observed for all **1-C*X*** samples (Fig. 3a). The small step located at ~390 nm derives from the absorption of lead bromide inorganic layers according to the previous study.[30] Contradictory to the similar absorption behavior, **1-C*X*** exhibits guest-dependent broadband emission (Fig. 3b) spanning the nearly whole visible range. The main peak gradually blue-shifts from 510 nm (**1-C1**) to 493 nm (**1-C5**), and then greatly red-shifts to ~550 nm when the water guest molecules are involved (**1-C6**, **1-C7**, and **1-C8**). To understand the influence of the dimeric configuration on the evolution of PL emission, the structure parameters including interplanar distance and overlap area are correlated with PL, as shown in Fig. 3c and d. Consistent with reported works,[37,40,41] the interplanar distance of An dimer shows unclear effects on the excimer formation in our case. Since a decent overlap of aromatic planes is required for excimer formation, a large overlap is expected to benefit the excimer formation.[37] As shown in Fig. 3d, the main peak blue shifts gradually from 510 nm (**1-C1**) to 493 nm (**1-C5**) concurrent with a decrease of overlap from 53.7% to 45.9%. This evolution is also observed for **1-C6**, **1-C7**, and **1-C8** with water guests. Nevertheless, this conclusion seems contradictory to the experimental results once taking all **1-C*X*** samples into account since **1-C*X*** ($6 \leq X \leq 8$) with a greater bathochromic emission show a smaller overlap relative to that of water-free **1-C*X*** ($1 \leq X \leq 5$). This motivates us to take a closer look into the overlap motifs (Fig. 3e), which can be indicated by the offset along the long (d_x) and short (d_y) axis of An molecules. The values of d_x are clustered into two groups including the range from 1.08 to 1.23 Å for **1-C*X*** ($6 \leq X \leq 8$) and 1.55–1.75 Å for **1-C*X*** ($1 \leq X \leq 5$). It has been calculated that a double-potential-well will be formed once An dimer is excited at the optimal geometry of ground states (S_0) with d_x = 1.3 Å.[4,39] As for **1-C*X*** ($6 \leq X \leq 8$) compounds with smaller d_x (1.08 Å $\leq d_x \leq$ 1.23 Å), all three anthracene rings participate in the π–π interaction, anthracene-type excimer is expected upon excitation, while naphthalene-type excimer is preferred for compounds with a larger d_x (1.55 Å $\leq d_x \leq$ 1.75 Å). Compared to naphthalene-type excimer, a larger charge-transfer (CT) contribution occurs for anthracene-type excimer, thereby leading to a greater bathochromic shift. Our experimental data are in good agreement with the calculated models.[4] Moreover, this conclusion is also applicable to solid-state **DCAn** and **(DCAn)Br**, further confirming the reasonability of this model.

Based on the above model, the value of d_y cannot change the types of the excimer, but tune the overlap. Therefore, d_y shows a similar effect as that of the overlap on the emission of An dimer, *i.e.*, smaller d_y results in a larger overlap and greater bathochromic shift (Fig. 3f). The PL lifetime tests further provide evidence to our speculation, as shown in Fig. S11.† All samples show a monoexponential decay and the time con-

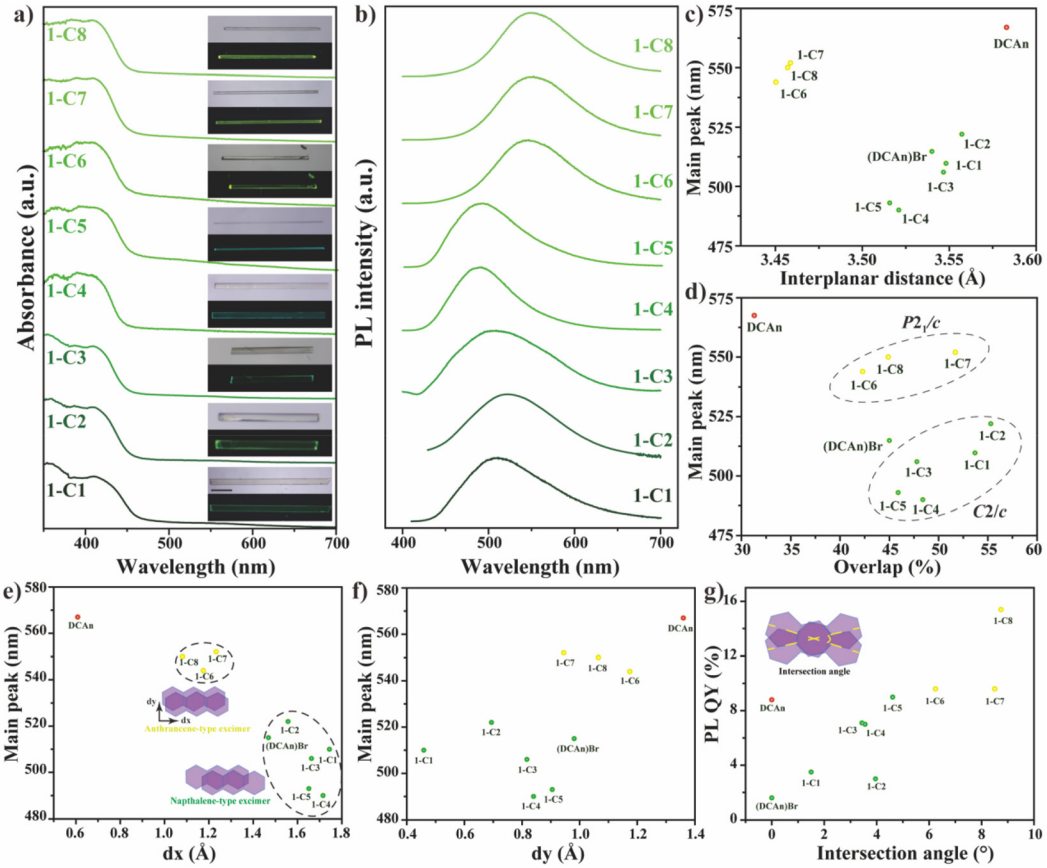

Fig. 3 (a) UV-vis and (b) PL spectra (λ_{ex} = 400 nm) of **1-C*X***. The correlation of the solid-state emission with (c) interplanar distance, (d) overlap ratio of An dimers, (e) the offset d_x, and (f) d_y. (g) Correlation of the PL QY with interplanar intersection angle.

stants can be separated into two groups including ~21 ns for **1-C*X*** ($1 \leq X \leq 5$) and 30 ns for **1-C*X*** ($6 \leq X \leq 8$), indicating the difference in excimer-types. Due to the larger CT contribution in anthracene-type excimer, **1-C*X*** ($6 \leq X \leq 8$) exhibits a larger degree of charge carrier delocalization, thus longer radiative lifetimes are expected.[42]

As a T-shaped molecule, the tertiary amine group of [**DCAn**]$^+$ is fixed through coulombic interaction and hydrogen bonding with inorganic layers, which only allows the fan-like swing of **DCAn** once increasing the intermolecular repulsion. As a result, the intersection angle of An dimer increases progressively from 1.502° (**1-C1**) to 8.742° (**1-C8**) upon decreasing the interplanar distance from 3.549 to 3.459 Å (Fig. 3g). It has been reported that H-aggregate (slide pitch angle > 54.7°) dimer will result in large energy splitting into the excited states, in which the lower one is optically forbidden.[43] In our case, the An dimers adopt the H-aggregated type for all **1-C*X*** samples, as evidenced by the low PL quantum yield (QY). Nevertheless, with the increase of the intersection angle, H-aggregated dimers gradually transform into X-aggregated type concurrent with the breaking of optically forbidden transition.[38] Therefore, PL QY (Fig. 3g) of **1-C*X*** monotonically increases from 3.5 (**1-C1**) to 15.4 (**1-C8**). **DCAn** seems to be an exception, which is probably ascribed to the unprotonated state.

Considering the weak interaction between the alcohol guest and **1-C*X*** host, we tried removing guest molecules by vacuum or heating activation to obtain a guest-free phase (**1-C*X***-act.). As shown in Fig. 4a, the XRD pattern of **1-C1**-act. shifts slightly towards a lower angle direction, verifying the increasing interlayer distance. The *T*-dependent XRD (Fig. S12†) also confirmed the generation of a new phase with a longer interlayer distance. Upon heating, a new diffraction peak rises on the left of the (002) peak until the complete transformation at 80 °C. Simultaneously, the removal of methanol guest causes a bathochromic shift of emission (Fig. 4b) from 510 (**1-C1**) to 543 nm (**1-C1**-act.), as evidenced by the color change of the logo pattern under UV irradiation (Fig. 4c). The guest-induced phase transformation and red-shift of emission are also observed for **1-C2** and **1-C3**. As shown in Fig. S13a,† both **1-C2**-act. and **1-C3**-act. show nearly identical PL spectra as that of **1-C1**-act., indicating the same stacking motif after activation. This result is consistent with the XRD patterns (Fig. S13b†), in which all diffraction peaks are well matched. However, the alcohol guests with longer lengths ($4 \leq X \leq 8$) cannot be removed through vacuum or heating activation, possibly attrib-

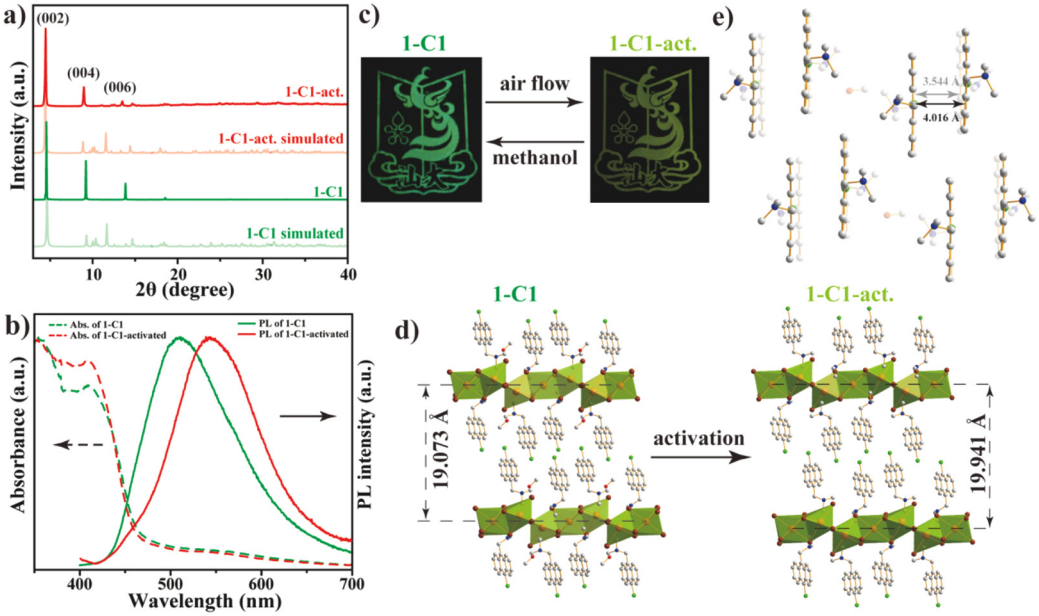

Fig. 4 (a) XRD patterns, (b) UV-vis and PL spectra of **1-C1** and **1-C1**-act. (c) The transformation of logo pattern under the irradiation of UV light after the treatment of airflow or methanol vapor. The variation of (d) crystal structures and (e) An dimers for **1-C1** and **1-C1**-act. simulated from DFT calculation. Pb (orange), Br (dark red), Cl (green), N (blue), O (red), and C (gray).

uted to the stronger guest–host interaction, higher boiling points, and larger volumes.

To understand the effect of methanol removal on the crystal structure and emission, the structure of guest-free **1-C1**-act. is optimized through density functional theory (DFT) calculation, as shown in Fig. 4d. Consistent with the XRD result (Fig. 4a), the crystal structure obtained through DFT calculation exhibits an apparent increase of interlayer distance from 19.073 to 19.941 Å after activation (Fig. 4d), confirming the reasonability of the optimized **1-C1**-act. structure. After removing methanol molecules, the interplanar distance of An cores increases to 4.016 Å (Fig. 4e). However, the variation of perpendicular distance looks contradictory to the great bathochromic shift of emission since the interplanar distance with 4.016 Å usually generates weaker excimer interaction.[11,37] Although the interplanar distance of An cores is increased, the removal of methanol guest also helps the transformation of An aggregates from dimeric to long-range stacking, which enhances the π–π interaction and exciton delocalization. This speculation can be confirmed by the *T*-dependent PL test of **1-C1**-act. and **1-C4**. As shown in Fig. S14,† the PL spectra of **1-C1**-act. gradually shift to a blue direction, while a red shift is observed for **1-C4** upon decreasing *T*. Such opposite behavior is ascribed to the different stacking motifs of the An aggregates. Since the butanol guest of **1-C4** cannot be removed through vacuum activation, lowering *T* will enhance the dimeric interaction of An, but weaken the long-range π–π interaction of **1-C1**-act.

DFT calculations (Fig. S15†) were conducted to better understand the electronic and band nature. Due to a large number of atoms and the limitation of computing resources, **1-C5**, and **1-C7** were chosen and compared. Although **1-C*X*** possesses similar structural features and components, a great difference in bandgap is observed for **1-C5** (1.41 eV) and **1-C7** (1.81 eV) with an indirect nature (Fig. S15a and c†). The total density of states (TDOS) of **1-C5** (Fig. S15b†) and **1-C7** (Fig. S15d†) show that the top of the valence band (VB) is primarily contributed by the inorganic components, while the bottom of the conduction band is mainly composed of C p states from An core. Since **1-C*X*** (*X* = 6, 7, 8) adopt a non-parallel orientation of An dimers, a weaker inter-dimer coupling of π-electrons and a more discrete energy level is expected. Therefore, the difference in bandgap possibly results from the various stacking modes of dimers in organic layers.

1-C*X* with rod-like morphology show bright emissive spots on the tips (Fig. 3a), indicating their potential in the optical waveguide.[44–47] As shown in Fig. 5a and b, both **1-C5** and **1-C7** show a high aspect ratio up to ~72 and the tips of all rod-shaped crystals exhibit much brighter spots under the irradiation of unfocused UV light. Such easily observed optical waveguide behavior motivates us to evaluate the optical loss coefficient. By varying the excitation laser beam (λ = 405 nm) at different positions of an individual 1D microcrystal (Fig. 5c), the spatially resolved PL images were obtained through near-field scanning optical microscopy (Fig. 5d and e). The intensity ratio between the tips and bodies (I_{tip}/I_{body}) against the propagation distance is fitted with a single-exponential function $I_{tip}/I_{body} = A\exp(-RD)$, where A is a constant, R is optical loss coefficient and D is the distance between the excited site and the emitting tip.[48,49] The R values were calculated to be 3.11 and 2.68 dB mm^{-1} for **1-C5** and **1-C7** (Fig. 5f and g), respectively, which are significantly smaller than most of the previously reported values for hybrid materials (Table S5†). Such

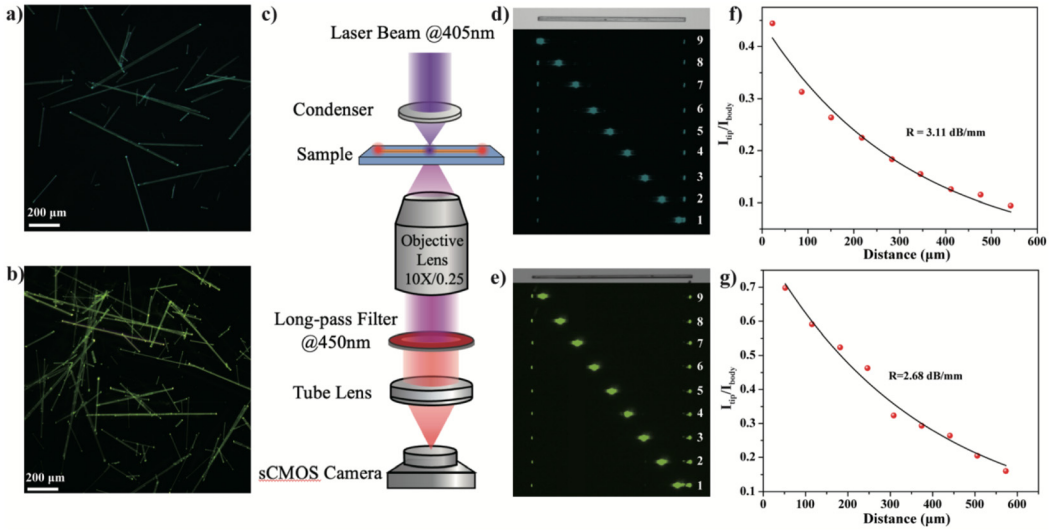

Fig. 5 PL microscope images of (a) **1-C5** and (b) **1-C7** under unfocused UV light (365 nm). (c) Schematic illustration of the optical waveguide test. PL microscope images of (d) **1-C5** and (e) **1-C7** for the optical waveguide test under the excitation of 405 nm continuous laser at different positions. The correlation of the I_{tip}/I_{body} with the photon propagation distance for (f) **1-C5** and (g) **1-C7**.

excellent performance is possibly ascribed to the high crystallization and emission with a large Stokes shift, which diminishes the effect of light scattering and reabsorption during propagation.

3. Conclusions

In summary, we have synthesized a series of 2D layered **1-C*X***, in which lead bromide inorganic layers function as the templates for the orientation of discrete An dimers spaced by straight alcohol guests. By varying the carbon chain length of guests, the stacking motifs and optical properties of An dimers can be widely tailored to unravel the key factors of the excimer formation. A closer look into the stacking motifs reveals that d_x value plays a key role in determining the excimer types. Smaller d_x benefits the formation of anthracene-type excimer with a larger CT content and greater bathochromic shift, while naphthalene-like excimer is preferred for d_x larger than 1.3 Å. Compared to the unclear role of interplanar distance, increasing the overlap ratio and decreasing d_y value help in strengthening the An excimer interaction. More importantly, rod-like **1-C*X*** crystals with a high aspect ratio of ~72 exhibit excellent performance on the optical waveguide. This work reports a new strategy to finely control the stacking configuration of molecular dimers and well understand the process of excimer formation in layered lead halide hybrids.

Author contributions

Conceptualization (B. Luo), data curation (X. Liu, X. Li, J. Li, Y. Xiao, Y. Kuai), formal Analysis (X. Liu, X. Li, B. Luo), funding acquisition (R. Zeng, W.-X. Ni, B. Luo), investigation (X. Liu, X. Li, J. Li, Y. Kuai), methodology (X. Liu, X. Li, K. Xu), DFT calculation (X. Lian, S. F. Ni), supervision (W.-X. Ni, Y. Kuai, B. Luo), writing (R. Zeng, B. Luo).

Conflicts of interest

The authors declare no competing financial interest.

Acknowledgements

This project was supported by Guangdong Basic and Applied Basic Research Foundation (2022A1515011997, 2022A1515110604), Guangdong Major Project of Basic and Applied Basic Research (2019B030302009), Li Ka Shing Foundation Cross-Disciplinary Research Project (2020LKSFG09A), Open Foundation of State Key Laboratory of Featured Metal Materials and Life-cycle Safety for Composite Structures (2022GXYSOF14) and Special Funds for the Cultivation of Guangdong College Students' Scientific and Technological Innovation (PDJH2021b0197). K. Xu thanks the financial support from National Natural Science Foundation of China (NSFC: 52203343).

References

1 H. Saigusa and E. C. Lim, Excimer Formation in Van Der Waals Dimers and Clusters of Aromatic Molecules, *Acc. Chem. Res.*, 1996, **29**, 171–178.
2 Y. Hong, J. W. Lam and B. Z. Tang, Aggregation-Induced Emission, *Chem. Soc. Rev.*, 2011, **40**, 5361–5388.

3 S. Yamane, Y. Sagara and T. Kato, Steric Effects on Excimer Formation for Photoluminescent Smectic Liquid-Crystalline Materials, *Chem. Commun.*, 2013, **49**, 3839–3841.
4 Y. Gao, H. Liu, S. Zhang, Q. Gu, Y. Shen, Y. Ge and B. Yang, Excimer Formation and Evolution of Excited State Properties in Discrete Dimeric Stacking of an Anthracene Derivative: A Computational Investigation, *Phys. Chem. Chem. Phys.*, 2018, **20**, 12129–12137.
5 A. Das, A. Danao, S. Banerjee, A. M. Raj, G. Sharma, R. Prabhakar, V. Srinivasan, V. Ramamurthy and P. Sen, Dynamics of Anthracene Excimer Formation within a Water-Soluble Nanocavity at Room Temperature, *J. Am. Chem. Soc.*, 2021, **143**, 2025–2036.
6 P. Nalaoh, N. Sungworawongpana, P. Chasing, W. Waengdongbung, P. Funchien, C. Kaiyasuan, T. Sudyoadsuk and V. Promarak, A Dimeric π-Stacking of Anthracene Inducing Efficiency Enhancement in Solid-State Fluorescence and Non-Doped Deep-Blue Triplet–Triplet Annihilation Organic Light-Emitting Diodes, *Adv. Opt. Mater.*, 2021, **9**, 2100500.
7 H. Osaki, *et al.*, A Macrocyclic Fluorophore Dimer with Flexible Linkers: Bright Excimer Emission with a Long Fluorescence Lifetime, *Angew. Chem., Int. Ed.*, 2016, **55**, 7131–7135.
8 S. Sekiguchi, K. Kondo, Y. Sei, M. Akita and M. Yoshizawa, Engineering Stacks of V-Shaped Polyaromatic Compounds with Alkyl Chains for Enhanced Emission in the Solid State, *Angew. Chem., Int. Ed.*, 2016, **55**, 6906–6910.
9 N. J. Hestand and F. C. Spano, Molecular Aggregate Photophysics Beyond the Kasha Model: Novel Design Principles for Organic Materials, *Acc. Chem. Res.*, 2017, **50**, 341–350.
10 S. Hu, *et al.*, Pressure-Induced Local Excitation Promotion: New Route toward High-Efficiency Aggregate Emission Based on Multimer Excited State Modulation, *J. Phys. Chem. Lett.*, 2022, **13**, 1290–1299.
11 Y. Hino, T. Matsuo and S. Hayashi, Structural Phase Transitions in Anthracene Crystals, *ChemPlusChem*, 2022, **87**, e202200157.
12 X. Shan, W. Chi, H. Jiang, Z. Luo, C. Qian, H. Wu and Y. Zhao, Monomer and Excimer Emission in a Conformational and Stacking-Adaptable Molecular System, *Angew. Chem., Int. Ed.*, 2022, e202215652.
13 J. Hoche, H. C. Schmitt, A. Humeniuk, I. Fischer, R. Mitric and M. I. S. Rohr, The Mechanism of Excimer Formation: An Experimental and Theoretical Study on the Pyrene Dimer, *Phys. Chem. Chem. Phys.*, 2017, **19**, 25002–25015.
14 H. Liu, *et al.*, Discrete Dimeric Anthracene Stackings in Solids with Enhanced Excimer Fluorescence, *Cryst. Growth Des.*, 2017, **17**, 2945–2949.
15 B. Luo, Y. Guo, Y. Xiao, X. Lian, T. Tan, D. Liang, X. Li and X. Huang, Fluorinated Spacers Regulate the Emission and Bandgap of Two-Dimensional Single-Layered Lead Bromide Perovskites by Hydrogen Bonding, *J. Phys. Chem. Lett.*, 2019, **10**, 5271–5276.
16 B. Luo, D. Liang, S. Sun, Y. Xiao, X. Lian, X. Li, M. D. Li, X. C. Huang and J. Z. Zhang, Breaking Forbidden Transitions for Emission of Self-Trapped Excitons in Two Dimensional $(F_2CHCH_2NH_3)_2CdBr_4$ Perovskite through Pb Alloying, *J. Phys. Chem. Lett.*, 2020, **11**, 199–205.
17 X. Li, X. Lian, J. Pang, B. Luo, Y. Xiao, M. D. Li, X. C. Huang and J. Z. Zhang, Defect-Related Broadband Emission in Two-Dimensional Lead Bromide Perovskite Microsheets, *J. Phys. Chem. Lett.*, 2020, **11**, 8157–8163.
18 Y. Tian, Y. Li, B. Chen, R. Lai, S. He, X. Luo, Y. Han, Y. Wei and K. Wu, Sensitized Molecular Triplet and Triplet Excimer Emission in Two-Dimensional Hybrid Perovskites, *J. Phys. Chem. Lett.*, 2020, **11**, 2247–2255.
19 Y. L. Lin and J. C. Johnson, Interlayer Triplet Energy Transfer in Dion-Jacobson Two-Dimensional Lead Halide Perovskites Containing Naphthalene Diammonium Cations, *J. Phys. Chem. Lett.*, 2021, **12**, 4793–4798.
20 B. Luo, Y. Guo, X. Li, Y. Xiao, X. Huang and J. Z. Zhang, Efficient Trap-Mediated Mn^{2+} Dopant Emission in Two Dimensional Single-Layered Perovskite $(CH_3CH_2NH_3)_2PbBr_4$, *J. Phys. Chem. C*, 2019, **123**, 14239–14245.
21 J. Wu, X. Li, X. Lian, B. Su, J. Pang, M. D. Li, Z. Xia, J. Z. Zhang, B. Luo and X. C. Huang, Ultrafast Study of Exciton Transfer in Sb(III)-Doped Two-Dimensional $[NH_3(CH_2)_4NH_3]CdBr_4$ Perovskite, *ACS Nano*, 2021, **15**, 15354–15361.
22 B. Su, S. Geng, Z. Xiao and Z. Xia, Highly Distorted Antimony(III) Chloride $[Sb_2Cl_8]^{2-}$ Dimers for Near-Infrared Luminescence up to 1070 nm, *Angew. Chem., Int. Ed.*, 2022, **61**, e202208881.
23 B. Su, G. Song, M. S. Molokeev, N. N. Golovnev, M. K. Lesnikov, Z. Lin and Z. Xia, Role of Metal-Chloride Anions in Photoluminescence Regulations for Hybrid Metal Halides, *J. Phys. Chem. Lett.*, 2021, **12**, 1918–1925.
24 X. Li, C. Peng, Y. Xiao, D. Xue, B. Luo and X.-C. Huang, Guest-Induced Reversible Phase Transformation of Organic–Inorganic Phenylpiperazinium Antimony(III) Chlorides with Solvatochromic Photoluminescence, *J. Phys. Chem. C*, 2021, **125**, 25112–25118.
25 Y. L. Lin, J. L. Blackburn, M. C. Beard and J. C. Johnson, Interlayer Triplet-Sensitized Luminescence in Layered Two-Dimensional Hybrid Metal-Halide Perovskites, *ACS Energy Lett.*, 2021, **6**, 4079–4096.
26 H. Hu, D. Zhao, Y. Gao, X. Qiao, T. Salim, B. Chen, E. E. M. Chia, A. C. Grimsdale and Y. M. Lam, Harvesting Triplet Excitons in Lead-Halide Perovskites for Room-Temperature Phosphorescence, *Chem. Mater.*, 2019, **31**, 2597–2602.
27 H. Hu, *et al.*, Efficient Room-Temperature Phosphorescence from Organic-Inorganic Hybrid Perovskites by Molecular Engineering, *Adv. Mater.*, 2018, e1707621.
28 U. Amrutha, A. Jesna and J. P. Jacob, Novel Diels–Alder Adducts Formed in the Reaction between a Few Anthracenemethanamines and Electron Deficient Dienophiles, *Chem. Data Collect.*, 2019, **23**, 100266.

29 J. Wang, J. Li, Q. Tan, L. Li, J. Zhang, J. Zang, P. Tan, J. Zhang and D. Li, Controllable Synthesis of Two-Dimensional Ruddlesden-Popper-Type Perovskite Heterostructures, *J. Phys. Chem. Lett.*, 2017, **8**, 6211–6219.
30 M. D. Smith, B. L. Watson, R. H. Dauskardt and H. I. Karunadasa, Broadband Emission with a Massive Stokes Shift from Sulfonium Pb–Br Hybrids, *Chem. Mater.*, 2017, **29**, 7083–7087.
31 O. P. Dimitriev, Y. P. Piryatinski and Y. L. Slominskii, Excimer Emission in J-Aggregates, *J. Phys. Chem. Lett.*, 2018, **9**, 2138–2143.
32 N. J. Hestand and F. C. Spano, Expanded Theory of H- and J-Molecular Aggregates: The Effects of Vibronic Coupling and Intermolecular Charge Transfer, *Chem. Rev.*, 2018, **118**, 7069–7163.
33 H. Liu, *et al.*, Monodisperse π-π Stacking Anthracene Dimer under Pressure: Unique Fluorescence Behaviors and Experimental Determination of Interplanar Distance at Excimer Equilibrium Geometry, *Adv. Opt. Mater.*, 2018, **6**, 1800085.
34 T. Eder, J. Vogelsang, S. Bange, K. Remmerssen, D. Schmitz, S. S. Jester, T. J. Keller, S. Hoger and J. M. Lupton, Interplay between J- and H-Type Coupling in Aggregates of pai π-Conjugated Polymers: A Single-Molecule Perspective, *Angew. Chem., Int. Ed.*, 2019, **58**, 18898–18902.
35 H. Liu, Y. Shen, Y. Yan, C. Zhou, S. Zhang, B. Li, L. Ye and B. Yang, One Stimulus in Situ Induces Two Sequential Luminescence Switchings in the Same Solvent-Fuming Process: Anthracene Excimer as the Intermediate, *Adv. Funct. Mater.*, 2019, **29**, 1901895.
36 Y. Shen, H. Liu, J. Cao, S. Zhang, W. Li and B. Yang, Unusual Temperature-Sensitive Excimer Fluorescence from Discrete π-π Dimer Stacking of Anthracene in a Crystal, *Phys. Chem. Chem. Phys.*, 2019, **21**, 14511–14515.
37 Y. Ge, Y. Wen, H. Liu, T. Lu, Y. Yu, X. Zhang, B. Li, S.-T. Zhang, W. Li and B. Yang, A Key Stacking Factor for the Effective Formation of Pyrene Excimer in Crystals: Degree of π–π Overlap, *J. Mater. Chem. C*, 2020, **8**, 11830–11838.
38 S. Ma, Y. Liu, J. Zhang, B. Xu and W. Tian, Polymorphism-Dependent Enhanced Emission in Molecular Aggregates: J-Aggregate Versus X-Aggregate, *J. Phys. Chem. Lett.*, 2020, **11**, 10504–10510.
39 T. Schillmöller, R. Herbst-Irmer and D. Stalke, Insights into Excimer Formation Factors from Detailed Structural and Photophysical Studies in the Solid-State, *Adv. Opt. Mater.*, 2021, **9**, 2001814.
40 Z. Zhang, Y. Zhang, D. Yao, H. Bi, I. Javed, Y. Fan, H. Zhang and Y. Wang, Anthracene-Arrangement-Dependent Emissions of Crystals of 9-Anthrylpyrazole Derivatives, *Cryst. Growth Des.*, 2009, **9**, 5069–5076.
41 P. Gayathri, S. Karthikeyan, M. Pannipara, A. G. Al-Sehemi, D. Moon and S. P. Anthony, Structural Insight of Anthracene Orientation by Halogen Substitution: Impact on Solid-State Fluorescence and Stimuli-Induced Fluorescence Switching, *Cryst. Growth Des.*, 2022, **22**, 5432–5440.
42 M. S. Myong, R. M. Young and M. R. Wasielewski, Excimer Diffusivity in 9,10-Bis(Phenylethynyl)Anthracene Assemblies on Anodic Aluminum Oxide Membranes, *J. Phys. Chem. C*, 2021, **125**, 24498–24504.
43 Q. Peng and Z. Shuai, Molecular Mechanism of Aggregation-Induced Emission, *Aggregate*, 2021, **2**, e91.
44 J. Zhao, T. Zhang, X. Y. Dong, M. E. Sun, C. Zhang, X. Li, Y. S. Zhao and S. Q. Zang, Circularly Polarized Luminescence from Achiral Single Crystals of Hybrid Manganese Halides, *J. Am. Chem. Soc.*, 2019, **141**, 15755–15760.
45 L. Lian, T. Zhang, H. Ding, P. Zhang, X. Zhang, Y.-B. Zhao, J. Gao, D. Zhang, Y. S. Zhao and J. Zhang, Highly Luminescent Zero-Dimensional Organic Copper Halide with Low-Loss Optical Waveguides and Highly Polarized Emission, *ACS Mater. Lett.*, 2022, **4**, 1446–1452.
46 B. Zhou, G. Xiao and D. Yan, Boosting Wide-Range Tunable Long-Afterglow in 1D Metal-Organic Halide Micro/Nanocrystals for Space/Time-Resolved Information Photonics, *Adv. Mater.*, 2021, **33**, e2007571.
47 X. Yang, L. F. Ma and D. Yan, Facile Synthesis of 1D Organic-Inorganic Perovskite Micro-Belts with High Water Stability for Sensing and Photonic Applications, *Chem. Sci.*, 2019, **10**, 4567–4572.
48 F. Liu, *et al.*, Light-Emitting Metal-Organic Halide 1D and 2D Structures: Near-Unity Quantum Efficiency, Low-Loss Optical Waveguide and Highly Polarized Emission, *Angew. Chem., Int. Ed.*, 2021, **60**, 13548–13553.
49 X. Yang, X. Lin, Y. Zhao, Y. S. Zhao and D. Yan, Lanthanide Metal-Organic Framework Microrods: Colored Optical Waveguides and Chiral Polarized Emission, *Angew. Chem., Int. Ed.*, 2017, **56**, 7853–7857.